Journal of Functional Foods 55 (2019) 184–192

Contents lists available at ScienceDirect

Journal of Functional Foods

journal homepage: www.elsevier.com/locate/jff

The effects of rooibos (*Aspalathus linearis*) on 3T3-L1 preadipocytes after the induction of mitochondrial dysfunction

Anna C. Hattingh*, Maryna van de Venter, Trevor C. Koekemoer

Department of Biochemistry and Microbiology, PO Box 77000, Nelson Mandela University, Port Elizabeth 6031, South Africa

ARTICLE INFO

Keywords:
Anti-ageing
Aspalathus linearis
Rooibos
3T3-L1 preadipocytes
Mitochondrial dysfunction
AMPK

ABSTRACT

Rooibos (*Aspalathus linearis*) is a South African fynbos plant, well-known for its strong anti-oxidant capacity and use in cosmetic products. The anti-ageing properties of fermented and green (unfermented) rooibos were investigated using a cell culture model designed to evaluate the involvement of mitochondrial dysfunction in the age-related decline in preadipocyte function. Mitochondrial dysfunction was induced through long-term exposure of 3T3-L1 preadipocytes to ethidium bromide (EtBr). Mitochondrial DNA (mtDNA) depleted (ρ^0) 3T3-L1 preadipocytes showed a significantly reduced rate of proliferation, delayed cell cycle progression (G0/G1 phase arrest), decreased mitochondrial membrane potential ($\Delta\Psi_m$), and increased glucose utilization and lactate production. Treatment with rooibos stimulated cell growth, attenuated G0/G1 phase arrest, improved $\Delta\Psi_m$, and increased glucose utilization and lactate production. Cellular ATP was significantly improved and AMPK activation was observed. The results obtained indicate that rooibos, particularly green rooibos, exhibit effects which preserve the functional capacity of preadipocytes exposed to ageing related insults.

1. Introduction

The natural process of ageing in multicellular organisms is associated with the progressive accumulation of deleterious changes in the functional capacity of biological systems, leading to an exponential decrease in the ability of cells to maintain homeostasis and ultimately increasing the probability of death (Ashok & Ali, 1999; Calabrese et al., 2012; Lui, Chen, Barnes, & Baron, 2010; Sohal & Orr, 2012). The free-radical hypothesis first proposed by Denham Harman in 1956 (Harman, 1956) has been considered as the most accepted and widely tested theory of ageing. Gradually it has evolved and been modified to include the concept of oxidative stress, and it is now believed that the process of ageing is induced, at least in part, by an imbalance between endogenous reactive oxygen species (ROS) and anti-oxidant defences (Calabrese et al., 2012).

As the main intracellular source of ROS, it is believed that mitochondria play a significant role in ageing and age-related diseases. Mitochondrial function declines with age, resulting in the impairment and/or alteration of mitochondria and any of its associated functions, including the inhibition of oxidative phosphorylation and respiration, mitochondrial network fragmentation, membrane depolarization, mitochondrial uncoupling or proton leak, ROS production, as well as the build-up of mitochondrial protein aggregates (Brand & Nicholls, 2011; Demine, Reddy, Renard, Raes, & Arnould, 2014; Pellegrino, Nargund, & Haynes, 2013). The consequences of mitochondrial dysfunction is as diverse as its cellular involvement, and it has been implicated in the process of ageing, as well as age-related neurodegenerative and metabolic diseases (Bratic & Larsson, 2013; Harman, 1972; Lagouge & Larsson, 2013; Page, Robb, Salway, & Stuart, 2010; Park & Larsson, 2011; Trifunovic & Larsson, 2008; Wallace, 2005; Yakes & Van Houten, 1997).

Changes in adipose tissue mass and distribution have been linked to mechanisms involved in longevity, age-related diseases and metabolic dysfunction (Sepe, Tchkonia, Thomou, Zamboni, & Kirkland, 2010; Tchkonia et al., 2010). The loss of subcutaneous adipose tissue predisposes to the development of altered cosmetic appearance (wrinkles, sunken eyes, skin folds), whereas the accumulation of visceral adipose tissue is associated with increased risk of age-related diseases, including those encompassed by the metabolic syndrome such as diabetes, hypertension, cancer, cognitive dysfunction, and atherosclerosis leading to heart attacks and strokes (Tchkonia et al., 2010). Recent studies have demonstrated that preadipocytes lose their ability to replicate and differentiate during ageing, and although the precise mechanisms involved remain to be established, it has been suggested that factors which are likely to contribute include mitochondrial dysfunction (Cartwright, Tchkonia, & Kirkland, 2007; Kusminski & Scherer, 2012;

* Corresponding author.
E-mail address: s207017852@mandela.ac.za (A.C. Hattingh).

https://doi.org/10.1016/j.jff.2019.02.017
Received 26 November 2018; Received in revised form 7 February 2019; Accepted 7 February 2019

Sepe et al., 2010; Tchkonia et al., 2010). Therefore, it is possible that preventing preadipocyte dysfunction may slow down or reverse age-related adipose dysfunction and its associated risks.

Treatment with anti-oxidants such as vitamin C, -E and polyphenols have been shown to be effective in improving resistance to oxidative stress, and subsequently prevent or attenuate cellular ageing (Baret et al., 2013; Masaki, 2010; Queen & Tollefsbol, 2010). Thus, it is not surprising that natural products rich in anti-oxidants have attracted remarkable interest in the cosmetic and pharmaceutical industry for its potential to restore and reverse the effects of ageing. Rooibos (*Aspalathus linearis* (Burm.f.), R. Dahlgren) is a robust fynbos plant endemic to the Cederberg Mountain region in the Western Cape of South Africa (Joubert & de Beer, 2011; Morton, 1983). Despite its increasing popularity as a value-added product in cosmetic products and its well-known anti-oxidant capacity, there exists little published research on its precise molecular and cellular involvement against ageing.

In this study an *in vitro* cell culture model, representative of the age-related mitochondrial dysfunction observed in preadipocytes, was established through the gradual depletion of mitochondrial DNA (mtDNA) achieved by long term exposure to sub-lethal concentrations of ethidium bromide (EtBr) (Amuthan et al., 2002; King & Attardi, 1989; Lim et al., 2006; Park & Lee, 2007; Schroeder, Gremmel, Berneburg, & Krutmann, 2008; Vankoningsloo et al., 2006). Mitochondrial dysfunction was subsequently evaluated and confirmed using known biochemical indicators including changes in survival n galactose medium, population doubling time, cell cycle distribution, mitochondrial membrane potential ($\Delta\Psi_m$), lactate production and glucose utilization. The potential anti-ageing properties of unfermented (green) and fermented rooibos (*Aspalathus linearis*) were then investigated by evaluating possible improvements using dysfunctional 3T3-L1 preadipocytes.

2. Materials and methods

2.1. Materials, reagents and chemicals

HyClone™ High glucose Dulbecco's modified Eagle's medium (DMEM), HyClone™ fetal bovine serum (FBS) and MitoTracker® Green FM were purchased from Thermo Scientific (GE Healthcare Life Sciences, Logan, Utah, USA). Galactose, Bovine Serum Albumin (BSA), 3,8-diamino-5-ethyl-6-phenylphenanthridinium bromide (Ethidium bromide, EtBr), bisBenzimide H 33342 trihydrochloride (Hoechst 33342), uridine, penicillin/streptomycin, phenol, glucose oxidase, lactate oxidase, peroxidase, 4-aminoantipyrine, 5,5′,6,6′tetrachloro-1,1′,3,3′-tetraethylbenzimidazol-carbocyanine iodide (JC-1) and valinomycin were all purchased from Sigma-Aldrich (St. Louis, MO, USA). The Coulter® DNA Prep™ and IntraPrep™ kits were purchased from Beckman Coulter (Brea, CA, USA). The CellTiter-Glo® 2.0 and CellTiter-Blue® assay reagents were obtained from Promega (Madison, WI, USA). Primary AMPKα (23A3) and p-AMPKα (Thr172) (40H9) rabbit monoclonal antibodies, and secondary anti-rabbit IgG (H + L), F(ab′)$_2$ Fragment (Alexa Fluor® 488 Conjugate) antibodies were all obtained from Cell Signalling Technology (Beverly, MA, USA).

2.2. Extracts

Fermented and green rooibos extracts were kindly provided by Prof. E. Joubert from the Post-Harvest and Wine Technology Division of the Agricultural Research Council of South Africa (ARC Infruitec-Nietvoorbij, Stellenbosch, South Africa), and used "as-is". The aspalathin-enriched green rooibos extract (GRE), also known as SB1/ARC2, was prepared according to a patented process described by Grüner-Richter, Otto, and Weinreich (2008), whereas the fermented rooibos extract (FRE), also known as ARC61, was prepared as described by Mazibuko et al. (2013). The phenolic composition of both extracts was previously characterised by HPLC-DAD (Mazibuko et al., 2013; Muller et al., 2012). The Pierce™ LAL Chromogenic Endotoxin Quantitation Kit (Thermo Scientific, USA), capable of detecting endotoxin levels as low as 0.1 endotoxin unit (EU)/mL or ± 0.01 ng endotoxin/mL, showed that both the fermented and green rooibos extracts were free of detectable endotoxins (data not shown).

2.3. Cell culture and establishment of ρ^0 3T3-L1 preadipocyte cell line

3T3-L1 mouse embryonic fibroblasts (ATCC® CL-173™), were maintained in DMEM (containing 4 mM L-glutamine, 25 mM glucose and sodium pyruvate) supplemented with 50 µg/mL uridine and 10% FBS at 37 °C in a humidified atmosphere with 5% CO_2. To generate mitochondrial DNA (mtDNA) depleted (ρ^0) cells, 3T3-L1 preadipocytes (referred to as wild type cells) were exposed to 50 ng/mL EtBr every day for a minimum of 10 passages (≥30 days) in complete medium (DMEM: 10% FBS) supplemented with 50 µg/mL uridine. Both wild type and ρ^0 3T3-L1 cells were concurrently maintained from passage number 10–25, and confluency not allowed to exceed 80%. To evaluate the mtDNA status of the EtBr treated cells, a representative sample (1×10^5) of cells was frequently sub-cultured in pyruvate free DMEM medium, without uridine and EtBr, and cell survival monitored. MtDNA depleted cells are characteristically auxotrophic for pyruvate and pyrimidines (uridine) and are therefore unable to survive in their absence (Wilkins, Carl, & Swerdlow, 2014; Yu et al., 2007). Subsequently, the inability of EtBr treated cells to survive in the absence of uridine served to confirm the depleted mtDNA status. No antibiotics were added during routine maintenance, however 1% (v/v) penicillin/streptomycin was added to long term experiments exceeding 5 days.

2.4. Experimental design

Rooibos extracts were freshly reconstituted prior to each experiment at a stock concentration of 40 mg/mL in dimethyl sulfoxide (DMSO), and diluted with complete medium to a working concentration of 100 µg/mL. Wild type and ρ^0 3T3-L1 cells were treated with 100 µg/mL green (GRE) and fermented (FRE) rooibos extracts for the indicated amount of time (24–48 h) to evaluate changes in cell characteristics after a more long-term exposure to treatments (i.e. changes resulting from gene/protein expression alterations). Natural repletion of mtDNA is reported to occur only after ± 7–12 days (Park & Lee, 2007; Seidel-Rogol, 2002), and therefore the mtDNA status of the ρ^0 3T3-L1 cells are considered to remain unaffected during 24–48 h treatment times. Included in each experiment was an untreated control, a vehicle control (0.25% DMSO in complete medium), as well as appropriate positive controls where relevant.

2.5. Cell viability and growth characteristics

Wild type and ρ^0 3T3-L1 cells were seeded at 10 000 cells/10 mL in 10 cm culture dishes. Cell number and viability was determined every day for 6 consecutive days using trypan blue exclusion and an automated cell counter, Luna™ (Logos Biosystems, Korea). Population doubling times were calculated during the most linear growth phases (48–120 h) using the formula:

$$DT = \frac{t\ln(2)}{\ln\frac{X_e}{X_b}}$$

X_e = Cell number at time point (t).
X_b = Cell number at t = 0

2.5.1. Cell viability in glucose/galactose medium

Wild type and ρ^0 3T3-L1 cells were seeded at 20 000 cells/mL in 200 µL aliquots in 96 well plates and left overnight to attach and recover. Cells were washed with phosphate buffered saline (PBS) and the culture medium replaced with either the usual complete medium

(DMEM, 25 mM glucose, 10% FBS) or DMEM substituted with 25 mM galactose instead of glucose. After 48 h of incubation, cell viability was determined using the CellTiter-Blue® assay. Fresh complete medium (containing glucose) was added to all wells, along with 20 µL of CellTiter-Blue®, and incubated for 4 h at 37 °C. Fluorescence (560Ex/590Em) was recorded using a BioTek® Synergy multi mode plate reader (Winooski, VT, USA).

2.6. Cell cycle analysis

Wild type and ρ^0 3T3-L1 cells were seeded at 30 000 cells/1.5 mL in 6 well culture dishes and left overnight to attach and recover. Cells were synchronised through serum deprivation overnight, after which the serum free medium was replaced with complete culture medium containing 10% FBS, to stimulate re-entry into the cell cycle.

Cells were collected by trypsinisation 24 and 48 h after adding the 10% FBS (in the absence of EtBr) and exposure to treatments. Cell suspensions (1 mL in PBS) were transferred into suitable polypropylene flow cytometry tubes (Beckman Coulter). The Coulter®DNA Prep™ kit was used for DNA cell cycle analysis, as per manufacturer's instructions. Briefly, cells were collected by centrifugation at 500 × g for 5 min at room temperature. A 100 µL aliquot of lysis reagent was added to each sample, vortexed and incubated for 5 min at room temperature. Thereafter, 500 µL propidium iodide (PI) (50 µg/mL) was added to the samples and incubated in the dark for 15 min at 37 °C, after which samples were analysed using a Beckman Coulter Cytomics FC500 Flow Cytometer. Data was recorded in FL3.

2.7. Mitochondrial membrane potential ($\Delta\Psi_m$)

Wild type and ρ^0 3T3-L1 cells were seeded at 30 000 cells/1.5 mL in 6 well culture dishes and left overnight to attach and recover. Changes in $\Delta\Psi_m$ were evaluated using the cytofluorimetric, lipophilic cationic dye JC-1. Cells were collected after 24 and 48 h of exposure to treatments (in the absence of EtBr) into polypropylene flow cytometry tubes, and JC-1 (1 mg/mL) was added to a final concentration of 2 µg/mL in pre-warmed, complete medium. Samples were incubated for 10 min in the dark at room temperature, after which three wash steps were performed using 500 µL PBS and centrifugation at 500*g* for 5 min. Red (FL3) and green (FL1) fluorescence was recorded using a Beckman Coulter Cytomics FC500 Flow Cytometer. Valinomycin, a K^+ ionophore, was used as a positive control due to its ability to dissipate the $\Delta\Psi_m$ (Felber & Brand, 1982).

2.8. Confocal microscopy

JC-1 (2.7) and MitoTracker® Green FM were used in conjunction with a Zeiss Axiovert LSM 510 META confocal microscope, equipped with a ZeissAxioCam camera for fluorescent imaging. The confocal microscope stage was also equipped with a specialized preheated (37 °C) humidified chamber supplied with 5% CO_2, thus enabling live cell imaging.

Wild type and ρ^0 3T3-L1 cells were seeded at 2000 cells/500 µL in specialized 35 mm glass bottom culture dishes to enable the use of higher objective imaging, and left overnight to attach and recover. JC-1 and MitoTracker® Green FM staining were performed according to manufacturer's instructions. Briefly, cells were incubated with pre-warmed complete culture medium containing either JC-1 (2 µg/mL) or MitoTracker® Green FM (20 nM) for 20 min, in the dark at 37 °C. The staining solutions were removed and cells were carefully washed using PBS. Fresh complete culture medium was added to the culture dishes, which were then allowed to equilibrate in the chamber for ± 10 min. A 488 nm laser line was used for excitation, along with appropriate band pass filters (CH2: BP 500–550 IR; CH3: BP 575–630 IR) to enable detection of green (CH2) and red (CH3) fluorescence emissions. High resolution static images, time lapse images, as well as optical slice (Z-stack) images taken at 1 µm intervals along the z axis, were acquired using a Plan-Apochromat 63× oil immersion objective (NA = 1.4). The laser light intensity and detector gains were set such that fluorescence intensities of the dyes were below saturation levels. Similarly, the pinhole size was kept constant throughout acquisition at 192 µm (CH2) and 220 µm (CH3) to avoid oversampling.

2.9. Metabolic parameters: Glucose utilization and lactate production

Assay reagents containing 3 mM phenol, 0.4 mM 4-aminoantipyrine, 2.5 mM EDTA, peroxidase, and either glucose oxidase or lactate oxidase in PBS (pH 7.4) were freshly prepared prior to each experiment. Wild type and ρ^0 3T3-L1 cells were seeded at 20 000 cells/mL in 200 µL aliquots in 96 well plates and left overnight to attach and recover. After 24 and 48 h of exposure to treatments, 5 µL of the culture medium was removed and added to 200 µL of the glucose oxidase and lactate oxidase assay reagents respectively. Samples were incubated for 10 min at 37 °C and the absorbance was recorded at 520 nm using a BioTek® PowerWave XS spectrophotometer (Winooski, VT, USA).

2.10. ATP content

Wild type and ρ^0 3T3-L1 cells were seeded at 20 000 cells/mL in 200 µL aliquots in white 96 well plates and left overnight to attach and recover. After 48 h of exposure to treatments, the CellTiter-Glo® 2.0 assay reagent was added according to manufacturer's instructions. Briefly, 100 µL of reagent was added to each well, the plate was placed on an orbital shaker for 2 min and then incubated in the dark for 10 min at room temperature. Luminescence was recorded using a BioTek® Synergy multi mode plate reader.

2.11. AMPK activation

Wild type and ρ^0 3T3-L1 cells were seeded at 20 000 cells/mL in 200 µL aliquots in 96 well plates and left overnight to attach and recover. After 48 h of exposure to treatments, the cells were fixed and permeabilised using the IntraPrep™ kit according to manufacturer's instructions. Cells were incubated with blocking buffer (0.5% BSA in PBS) and thereafter incubated with the antibodies separately (1:100 for AMPKα and 1:100p-AMPKα) for 1 h at 37 °C. Cells were washed and incubated with the conjugated secondary antibody (1:1000) for 30 min at 37 °C in the dark. Cells were washed and stained with Hoechst 33342 (1 µg/mL) in PBS for 30 min. Fluorescent micrographs were acquired using an ImageXpress® Micro XLS wide-field high content analysis system (Molecular Devices, San Jose, CA, USA). Nine image sites were acquired per well using a 10× objective and appropriate DAPI and FITC filter sets.

2.12. Data analysis and statistics

Unless otherwise stated, each experiment was performed in triplicate and repeated 3 independent times (n = 3). Results are expressed as mean ± standard deviation (SD). Statistical significance was determined using the two-tailed student's *t*-test where $p \leq 0.05$ (*) and $p \leq 0.005$ (**) were considered significant. For flow cytometry, a minimum of 10 000 gated events were recorded for each sample and results and histograms obtained were analysed using FlowJo v10 software (Tree Star Inc., USA). Post-acquisition confocal microscopy image processing was performed using ZEN 2012 software (Carl Zeiss Microscopy GmbH, 2011). Fluorescent micrographs were analysed using the Multi-wavelength cell scoring module from MetaXpress® High-Content Image Acquisition and Analysis Software (Version 6.1, Molecular Devices, San Jose, CA, USA).

Table 1
Comparison of wild type (wt) and ρ^0 3T3-L1 preadipocyte cell characteristics.

	wt	ρ^0
Population doubling time (h)	18.8 ± 2.10	30.2 ± 4.20**
Cell cycle analysis (% cell population in G1/G0 phase)	42.2 ± 2.78	49.0 ± 2.70**
Cell viability in glucose medium[b] (% relative to wt control)	–	98.2 ± 3.80
Cell viability in galactose medium[b] (% relative to wt control)	–	15.5 ± 1.03**
Mitochondrial membrane potential ($\Delta\Psi_m$) Mean fluorescent intensity ratio (FL3/FL1)[a]	1.50 ± 0.69 + *Valinomycin* 0.564 ± 0.08*	1.02 ± 0.50* + *Valinomycin* 0.316 ± 0.05**
Mitochondrial mass[c] Mean fluorescent intensity	42.72 ± 7.01	42.19 ± 5.97
Glucose utilization[b] (% increase relative to wt control)	–	18.0 ± 2.32**
Lactate production[b] (% increase relative to wt control)	–	57.8 ± 3.93**
AMPK activation (% increase in p-AMPK relative to wt control)	–	14.6 ± 18.6
ATP content[b] (% relative to wt control)	–	47.8 ± 4.23**

Summary data are shown as the mean ± standard deviation of three independent experiments, each performed in triplicate (n = 3).
Each parameter was compared for significant differences between wild type and ρ^0 cells using the student's *t*-test where $p \leq 0.05$ (*) and $p \leq 0.005$ (**) were considered significant.

[a] Mean fluorescent intensity ratio. Mitochondrial depolarization is accompanied by a decrease in red (FL3)/green (FL1) fluorescence intensity ratio.

[b] Results normalised relative to cell density.

[c] Mitochondrial mass indicated by the mean fluorescence intensity of MitoTracker® Green FM determined during live cell imaging using confocal microscopy (63× oil immersion magnification).

3. Results

3.1. Generation and characterization of ρ^0 3T3-L1 preadipocytes

After continuous, long term exposure of 3T3-L1 preadipocytes to 50 ng/mL EtBr, mtDNA depleted (ρ^0) 3T3-L1 cells were generated and subsequently characterised through biochemical indicators of mitochondrial dysfunction including changes in cell growth characteristics, survival in galactose medium, population doubling time, cell cycle distribution, mitochondrial mass and membrane potential ($\Delta\Psi_m$), ATP content, lactate production and glucose utilization (Table 1).

P^0 3T3-L1 cells exhibited a significantly reduced growth rate, as illustrated by the increased population doubling time (30.2 ± 4.2 h) compared to wild type cells (18.8 ± 2.1 h), as well as the delay in cell cycle progression - indicated by a 16% increase in the number of cells remaining in the G1/G0 phase relative to wild type cells. Cell viability, determined by trypan blue exclusion, remained unaffected throughout EtBr treatment (data not shown). However, ρ^0 3T3-L1 cells suffered a progressive decline in cell number over several days once pyruvate and uridine were removed from the cell culture medium (data not shown). Auxotrophic reliance on pyruvate and uridine is commonly associated with ρ^0 cells, and this simple test is considered a useful indicator of the cellular respiratory status and mtDNA content of ρ^0 cells (Wilkins et al., 2014; Yu et al., 2007). Furthermore, wild type 3T3-L1 cells exhibited no change in cell viability when glucose was substituted with galactose as the sole sugar source in the culture medium, whereas ρ^0 3T3-L1 cell viability decreased to 15.5% after 48 h. Replacing glucose with galactose in the culture medium, forces cells to rely on mitochondrial oxidative phosphorylation to generate sufficient cellular ATP for survival and is commonly used to diagnose mitochondrial toxicity and dysfunction (Dykens, Marroquin, & Will, 2007; Gohil et al., 2011; Komulainen et al., 2015).

Metabolic alterations became visibly apparent as a progressive increase in acidification of the cell culture medium (indicated by the colour change of the pH indicator phenol red) was observed during routine maintenance of ρ^0 3T3-L1 cells. This was attributed to an increase in lactate production, which was confirmed by the ± 57.8% increase in lactate production observed relative to wild type cells.

Depletion of mtDNA, encoding complex I, III, and IV of the respiratory chain, results in dysfunctional mitochondrial respiration and oxidative phosphorylation, thereby constraining the cell to use alternative energy generation pathways such as glycolysis. The overreliance on this more inefficient ATP generating process results in a significantly increased demand for glucose, which was evident in the ± 18% increase in glucose utilization relative to wild type cells. Furthermore, mtDNA depletion and subsequent reduction in the transfer of electrons from NADH to O_2 results in a severe decrease in the NAD/NADH ratio which will ultimately restrict glycolysis unless NAD is regenerated. The conversion of pyruvate to lactate by lactate dehydrogenase serves to regenerate NAD and thus sustain the elevated glycolytic flux in mtDNA depleted cells. Elevated glucose consumption and lactate production are thus often used as markers to indicate mitochondrial health/dysfunction (Kemppainen et al., 2016). The decreased ATP content (47.8% relative to wild type cells) further supports a less efficient capacity to generate ATP in the ρ^0 cells. Although the expected increase in AMPK phosphorylation and activation can be observed in ρ^0 cells relative to wild type cells, this result was not statistically significant.

Mitochondrial depolarization is indicated by a decrease in the red/green fluorescence intensity ratio of JC-1, independent of changes in mitochondrial size, shape or density. A ± 32% decrease in mitochondrial membrane potential ($\Delta\Psi_m$) was observed relative to wild type cells and treatment with Valinomycin resulted in a 62.4% and 69% decrease in $\Delta\Psi_m$ for both wild type and ρ^0 3T3-L1 cells, respectively. This significant decrease in $\Delta\Psi_m$ indicates that EtBr treatment negatively affects mitochondrial health, mimicking the aged phenotype, without affecting cell viability - considering that cell viability remained unaffected throughout exposure to EtBr and cells retained their ability to proliferate, albeit at a much-reduced rate. Maintenance of a low $\Delta\Psi_m$ in the absence of respiration has frequently been observed in other ρ^0 cell lines and is said to be due to the reversed action of adenine nucleotide translocator (ANT) in combination with F1-ATPase activity (Arnould et al., 2003; Buchet & Godinot, 1998).

MitoTracker® Green FM accumulates in the mitochondria irrespective of $\Delta\Psi_m$ and is

commonly used to determine and observe mitochondrial mass, morphology and distribution (Cottet-Rousselle, Ronot, Leverve, & Mayol, 2011; Pendergrass, Wolf, & Poot, 2004; Stankov, Lücke, Das, Schmidt, & Behrens, 2010). Fluorescence intensities, indicating the accumulation of MitoTracker® Green FM within the mitochondria, was determined from images acquired using confocal microscopy and Zen software post-acquisition processing. Using 10 randomly selected cells from both the wild type and ρ^0 3T3-L1 cell populations, the mean fluorescence intensity ± SD obtained for ρ^0 3T3-L1 cells (42.19 ± 5.97) indicated no significant change relative to that obtained for the wild type cells (42.72 ± 7.01). This is in accordance with findings by Armand et al. (2004), Holmuhamedov, Jahangir, Bienengraeber, Lewis, and Terzic (2003), Gilkerson, Margineantu, Capaldi, and Selker (2000) and Kukat et al. (2008), indicating that mtDNA depletion does not affect the number or biogenesis of mitochondria.

3.2. Effect of rooibos on ρ^0 3T3-L1 preadipocytes

The potential anti-ageing properties of green (GRE) and fermented (FRE) rooibos extracts were investigated using ρ^0 3T3-L1 preadipocytes, representative of mitochondrial dysfunction, a characteristic associated with the age related decline in preadipocyte function (Kusminski & Scherer, 2012). The effects of rooibos on cell growth and proliferation,

Table 2
Summary of cell cycle analysis results obtained after treatment of ρ^0 3T3-L1 preadipocytes with GRE and FRE (100 µg/mL). Cell cycle analysis was performed using PI staining 24 and 48 h after re-entry into the cell cycle following synchronization through serum deprivation.

		ρ^0	GRE	FRE
24 h	Sub-G1	2.43 ± 1.53	1.68 ± 0.35	2.56 ± 0.66
	G1/G0	48.8 ± 3.34	42.0 ± 0.83**	47.1 ± 2.17
	S	18.8 ± 3.02	18.3 ± 1.45	17.1 ± 1.87
	G2/M	23.2 ± 2.68	32.0 ± 2.63**	28.1 ± 1.77*
48 h	Sub-G1	2.02 ± 0.46	2.61 ± 0.43	2.68 ± 1.11
	G1/G0	49.0 ± 2.70	52.4 ± 5.60	59.8 ± 4.92**
	S	13.3 ± 3.47	16.8 ± 3.91	15.0 ± 4.80
	G2/M	31.7 ± 2.15	24.3 ± 2.95**	18.9 ± 3.36**

Values indicate mean % ± SD of three independent experiments, each performed in triplicate (n = 3). Statistical significance was determined using the two-tailed Student *t*-test and is indicated for $p \leq 0.05$ (*) and $p \leq 0.005$ (**) relative to the untreated ρ^0 control.

$\Delta\Psi_m$, metabolic parameters such as glucose utilization and lactate production, ATP content and AMPK activation were evaluated.

3.2.1. Cell growth characteristics

A significant increase in cell density is observed after 24 h of treatment with GRE, although this effect becomes less pronounced after 48 h. Although FRE seems to indicate a possible increase in cell density over 24 and 48 h, these changes were not statistically significant. This is congruent to population doubling times indicating no effect after FRE treatment (30.3 ± 4.9 h) and a slight improvement after GRE treatment (28.0 ± 3.7 h) relative to ρ^0 3T3-L1 controls (30.2 ± 4.2 h), however results remained markedly higher relative to the wild type controls (18.8 ± 2.1 h).

3.2.2. Cell cycle analysis

Cell cycle analysis was performed on synchronised rooibos treated and untreated ρ^0 3T3-L1 cells after 24 and 48 h. A summary of the percentage cells present in each cell cycle phase is presented in Table 2.

Considering that ρ^0 3T3-L1 cells generally exhibit a delay in G1-S phase transition (Table 1), the significant decrease (6.8%) in the number of cells in the G1/G0 phase after 24 h of treatment with GRE, along with a concurrent increase (8.8%) in the number of cells present in the G2/M phase, indicates that the rooibos treatment stimulated cell cycle progression. A similar but less significant effect is observed for FRE treated cells. However, after 48 h of treatment with GRE and FRE, a complete change in the cell cycle distribution is seen due to the increase in the number of cells present in the G1/G0 phase as well as the S phase, compared to a significant decrease in the number of cells present in the G2M phase. Although more difficult to interpret due to the 48 h time period after synchronisation, these results are in accordance with the increased proliferation and cell density observed after 24 h of treatment with GRE (Fig. 1).

3.2.3. Mitochondrial membrane potential ($\Delta\Psi_m$)

The effect of rooibos treatment on the $\Delta\Psi_m$ was determined using the lipophilic cationic dye JC-1, which exhibits a potential-dependent accumulation in the mitochondria. JC-1 will either be retained in the mitochondria due to the negative charge, established by the intact $\Delta\Psi_m$, and form J-aggregate complexes emitting a red fluorescence (polarised mitochondria), or will diffuse into the cytoplasm due to a collapse in $\Delta\Psi_m$, where the monomeric form will exhibit a green fluorescence (depolarised mitochondria).

As shown in Fig. 2 an initial decrease of ± 30% in $\Delta\Psi_m$ was observed after 24 h of treatment with GRE. At 48 h, the $\Delta\Psi_m$ was restored to the same level as that of the untreated ρ^0 3T3-L1 control. Increased polarization of the mitochondrial membrane is observed after 48 h of treatment with FRE.

3.2.4. Confocal microscopy

To confirm and visualise the $\Delta\Psi_m$ changes observed with flow cytometry (Section 3.2.3), rooibos treated ρ^0 3T3-L1 cells were stained with JC-1 and analysed using confocal microscopy and Zen software post-acquisition processing. One representative of 15 images taken for each respective treatment, during a single experiment is shown in Fig. 3. A ratio of red/green fluorescence intensity, indicating the $\Delta\Psi_m$, was determined for 10 randomly selected cells exposed to either GRE or FRE for 48 h.

During the progression of the cell cycle, mitochondria undergo changes in morphology, size, distribution and abundance (Arakaki et al., 2006; Ferree & Shirihai, 2012). This morphological spectrum has been characterised according to the cell cycle progression into tubular, intermediate and fragmented conformations (Margineantu et al., 2002; Mitra, Wunder, Roysam, Lin, & Lippincott-Schwartz, 2009). As can be seen in Fig. 3, a primarily fragmented mitochondrial distribution was observed in ρ^0 3T3-L1 cells, indicating G1 arrested or G0 phase cells, which is consistent with the results obtained for cellular growth characteristics and cell cycle analysis (Table 1). This is in accordance with findings by Arduíno et al. (2012); Margineantu et al. (2002) and Minamikawa et al. (1999) indicating similar trends in mitochondrial morphology and distribution for mtDNA depleted 143B osteosarcoma cells and NT2 teratocarcinoma cells. GRE and FRE treated ρ^0 3T3-L1 cells have a more intermediate mitochondrial arrangement, typical of proliferating cells (G1-S or S phase), with tubular elements clearly visible.

3.2.5. Metabolic parameters: Glucose utilization and lactate production.

Given that glucose metabolism is strongly correlated to mitochondrial function, glucose utilization and lactate production (Fig. 4) were investigated as markers for changes in mitochondrial function upon treatment with rooibos.

Relative to wild type cells, ρ^0 3T3-L1 cells demonstrated a marked

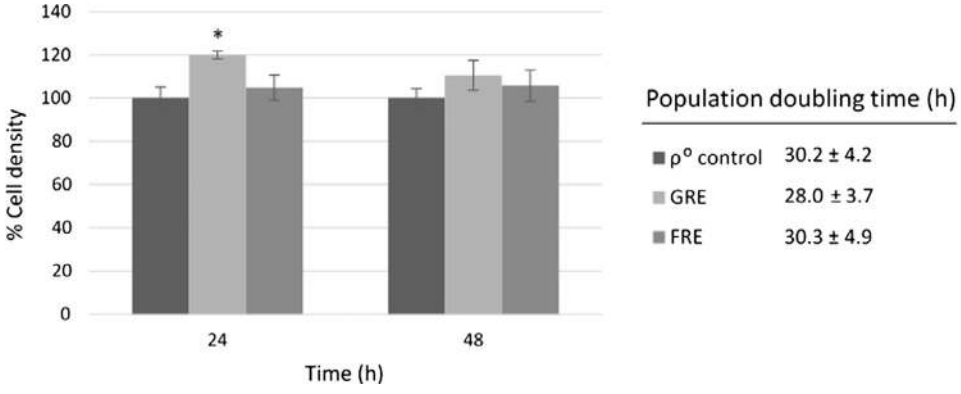

Fig. 1. Effect of GRE and FRE (100 µg/mL) on cell density and population doubling time of ρ^0 3T3-L1 preadipocytes. Cell density was determined using the Luna™ automated cell counter (Logos Biosystems, Korea) and is represented as a percentage of the total viable cell number relative to the ρ^0 control (100%). Error bars represent SD of four independent experiments, each performed in triplicate (n = 4). Statistical significance was determined using the two-tailed Student *t*-test and is indicated for $p < 0.05$ (*) relative to the ρ^0 control.

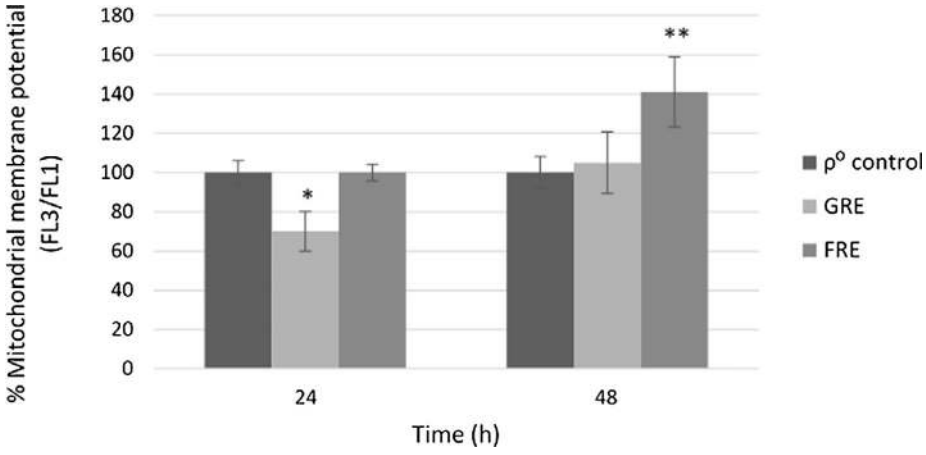

Fig. 2. Effect of GRE and FRE (100 μg/mL) on the mitochondrial membrane potential of ρ^0 3T3-L1 preadipocytes. Cells were stained with the polychromatic, $\Delta\Psi_m$ sensitive probe JC-1. The $\Delta\Psi_m$ is represented as the ratio of the mean fluorescence intensity of FL3 (red) to FL1 (green). Error bars represent SD of three independent experiments, each performed in triplicate (n = 3). Statistical significance was determined using the two-tailed Student *t*-test and is indicated for $p < 0.05$ (*) and $p < 0.005$ (**) relative to untreated ρ^0 control. (For interpretation of the references to colour in this figure legend, the reader is referred to the web version of this article.)

increase in glucose utilization after treatment with GRE and FRE, with GRE treatment resulting in a ± 25.8% increase which remains unchanged after 48 h, and FRE treatment resulting in a ± 7.76% and ± 20.2% increase after the respective 24 and 48 h treatments. Lactate production was significantly decreased after 24 and 48 h of GRE and FRE treatment, thus indicating a decrease in the reliance on glycolysis to supply the ATP needs of these mitochondrially depleted cells (Table 1). This is in accordance with numerous other studies which have demonstrated that rooibos (green and fermented) treatment increases glucose uptake in mitochondrial competent cells (Joubert & de Beer, 2011; Muller et al., 2012; Sanderson et al., 2014). It is, however, difficult to distinguish between metabolic alterations arising from direct effects on mitochondrial dysfunction *per se* and that resulting from any other metabolic perturbation in response to rooibos treatment.

Although the decreased lactate production upon treatment with GRE and FRE suggests a decreased requirement for NAD regeneration and consequently an improvement in mitochondrial function, corresponding glucose consumption remains increased, in contrast arguing in favour of an increased reliance on glycolytic ATP production and thus a decline in mitochondrial capacity. The significant decrease in $\Delta\Psi_m$ in GRE treated ρ^0 3T3-L1 cells argues in favour of a weaker mitochondrial function while improvements in the growth characteristics are in line with an improved mitochondrial function.

3.2.6. ATP content

To further investigate the apparent discrepancy in glucose utilization and lactate production, cellular ATP content of FRE and GRE treated ρ^0 cells were measured (Fig. 5). After 48 h of treatment with both GRE and FRE, a significant increase in ATP content can be observed relative to the ρ^0 3T3-L1 control (13.6% and 24.8%, respectively).

3.2.7. AMPK activation

AMPK is an important coordinator of many age-related signalling pathways, correspondingly increased AMPK activity has been shown to extend the lifespan of lower model organisms (Salminen & Kaarniranta, 2012). Previous studies have already shown that rooibos can activate AMPK (Mazibuko et al., 2013) thus, it was important to evaluate the effect of GRE and FRE on ρ^0 3T3-L1 cells (Fig. 6). After 48 h an increase in phosphorylation of basal AMPK was observed for GRE (2.04 ± 0.30) and FRE (2.17 ± 0.31) treated cells relative to untreated ρ^0 3T3-L1 cells (1.61 ± 0.26), suggesting an improvement in the cellular energy status and thus corroborating changes observed for ATP levels.

4. Discussion

In this study, a ρ^0 3T3-L1 preadipocyte cell line was successfully established through exposure to 50 ng/mL EtBr for ± 30 days. EtBr is a cationic phenanthridine dye that binds to, and intercalates with, double stranded DNA through electrostatic interactions (Das, Parveen, & Pradhan, 2014; Khan, Smigrodzki, & Swerdlow, 2007). Its positive charge allows it to preferentially accumulate within the negatively charged mitochondria, where it inhibits replication and transcription of mitochondrial DNA (mtDNA) subsequently leading to the gradual depletion of mtDNA without significantly affecting nuclear DNA (Khan et al., 2007; King & Attardi, 1989). Although the complete mechanism of action and effects of EtBr treatment on other aspects of cell integrity remains to be established, using EtBr to deplete mtDNA remains a popular method to generate ρ^0 cells (van Gisbergen et al., 2015; Warren, Aicher, Fessel, & Konradi, 2017).

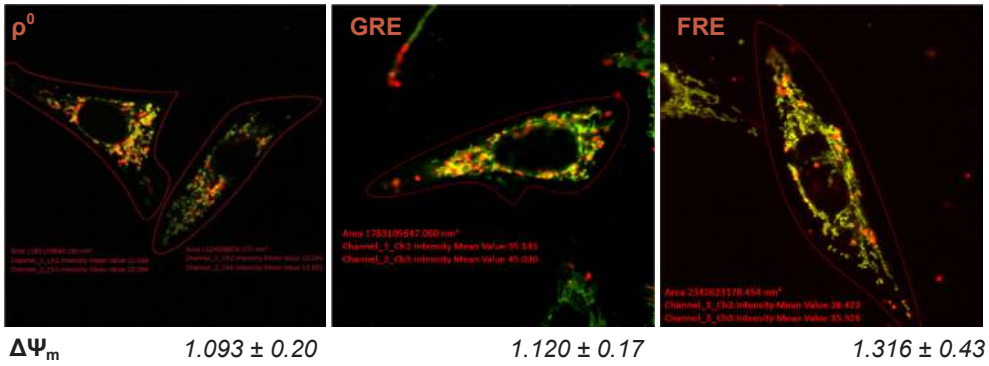

Fig. 3. Representative confocal microscopy images of JC-1 stained mitochondria in ρ^0 3T3-L1 preadipocytes after 48 h treatment with GRE and FRE (100 μg/mL). Live cell imaging was performed using confocal microscopy (63× oil immersion magnification). JC-1 is a polychromatic $\Delta\Psi_m$ sensitive fluorescent probe, exhibiting $\Delta\Psi_m$ accumulation and aggregate formation within the mitochondria. Polarized (red) and depolarized (green) mitochondria are indicated with yellow colouration representing overlap. One representative of 10 images taken for each respective cell population, during a single experiment. (For interpretation of the references to colour in this figure legend, the reader is referred to the web version of this article.)

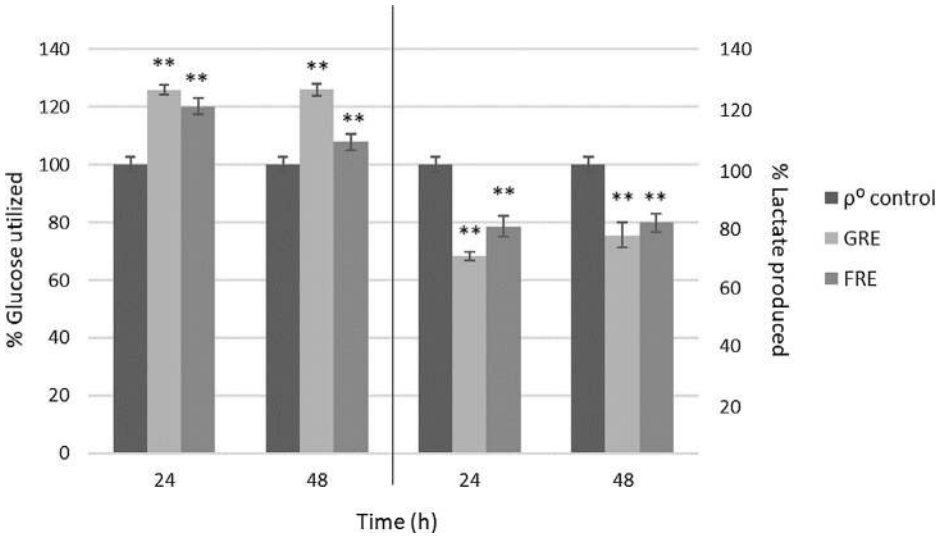

Fig. 4. Effect of GRE and FRE (100 μg/mL) on glucose utilization and lactate production of ρ^0 3T3-L1 preadipocytes. Error bars represent SD of three independent experiments, each performed in triplicate (n = 3). Statistical significance was determined using the two-tailed Student *t*-test and is indicated for $p < 0.05$ (*) and $p < 0.005$ (**) relative to untreated ρ^0 control, and normalised relative to cell density.

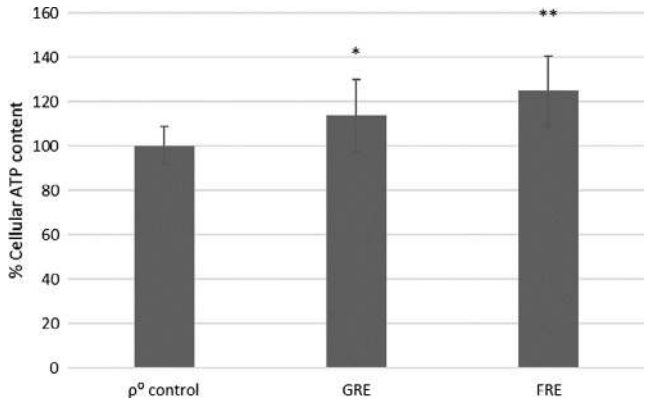

Fig. 5. Effect of GRE and FRE (100 μg/mL) on the ATP content of ρ^0 3T3-L1 preadipocytes after 48 h of treatment. Error bars represent SD of three independent experiments, each performed in triplicate (n = 3). Statistical significance was determined using the two-tailed Student *t*-test and is indicated for $p < 0.05$ (*) and $p < 0.005$ (**) relative to untreated ρ^0 control, and normalised relative to cell density.

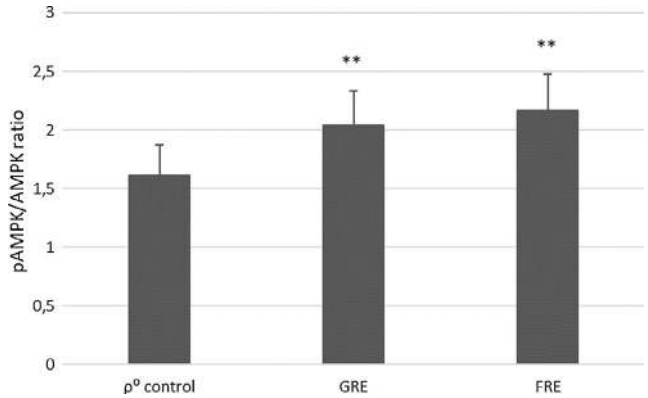

Fig. 6. Effect of rooibos (100 μg/mL) on AMPK activation in ρ^0 cells. The ratio of pAMPK: AMPK is shown as a measure of AMPK activation. Error bars represent SD of three independent experiments, each performed in triplicate (n = 3). Statistical significance was determined using the two-tailed Student *t*-test and is indicated for $p < 0.005$ (**) relative to untreated ρ^0 control.

Relative to wild type 3T3-L1 preadipocytes, ρ^0 3T3-L1 preadipocytes exhibited a significantly reduced growth rate, as illustrated by the substantially increased population doubling time as well as delayed cell cycle progression. This is in accordance with findings by Lim et al. (2006) using C2C12 myotubes, and Yu et al. (2007) using T47D human breast cancer cells. The reliance on external supplementation of pyruvate and uridine can be attributed to dysfunctional mitochondrial respiration and oxidative phosphorylation (Armand et al., 2004; Magda et al., 2008; Yu et al., 2007). Uridine dependence is attributed to inactive dihydroorotate dehydrogenase, an enzyme that relies on the activity of the electron transport chain to catalyse the conversion of dihydroorotic acid to orotic acid and following downstream processes to produce uridine (Khan et al., 2007). Similarly, pyruvate auxotrophy is a result of a compensatory overreliance on glycolysis to produce cellular energy, thereby leading to increased accumulation of cytosolic NADH (Armand et al., 2004; Khan et al., 2007; Yu et al., 2007). Excess pyruvate can therefore assist in the regeneration of NAD through the conversion of pyruvate to lactate via lactate dehydrogenase. This change in metabolic function was confirmed by the significantly increased glucose consumption and lactate production of ρ^0 3T3-L1 cells relative to wild type cells.

P^0 3T3-L1 cells progressed through the cell cycle much slower than wild type cells, as indicated by the significantly increased number of cells remaining in the G1/G0 phase, as well as the reciprocal reduction in the number of cells present in the S phase after 24 and 48 h (Table 1). These results may be attributed to the activation of the mitochondrial damage check point or mitocheckpoint, which will permit cells to arrest in the cell cycle and repair some mitochondrial function in order to avoid apoptosis (Singh, 2004; Yu et al., 2007). Additionally, reduced mitochondrial dynamics and bioenergetics associated with mitochondrial dysfunction could also be a contributing factor due to the fact that mitochondria are required to coalesce into a large hyperpolarised, hyperfused tubular network prior to the transition from G1 to S phase (Finkel & Hwang, 2009; Mitra et al., 2009). Mitochondrial morphology and distribution observed through confocal microscopy indicated a fragmented mitochondrial distribution in ρ^0 3T3-L1 cells, further indicating G1 arrested or G0 phase cells. Mitochondrial membrane potential ($\Delta\Psi_m$), established through the activity of oxidative phosphorylation, is an important indicator of mitochondrial function and the overall health status of a cell. The significantly decreased $\Delta\Psi_m$ observed for ρ^0 3T3-L1 cells was insufficient to induce cell death, supported by the observation that cell viability and sub-G1 phase cell populations were unaffected by EtBr treatment. ATP content in ρ^0 3T3-L1 cells was also significantly reduced, supporting the results obtained for $\Delta\Psi_m$ as well as glucose utilization and lactate production. P^0 cells are thought to maintain their low $\Delta\Psi_m$ through consumption of ATP in their mitochondria as a result of the reversed action of ANT in combination with F1-ATPase activity (Chandel & Schumacker, 1999). Collectively,

the above data confirmed that 3T3-L1 preadipocytes treated with EtBr produced an *in vitro* cell culture model representative of mitochondrial dysfunction as a consequence of the proposed effect of EtBr treatment on mtDNA. Furthermore, the growth and biochemical characteristics of these mitochondrial dysfunctional cells reflect that of ageing adipose tissue preadipocytes and therefore provide a suitable model to investigate potential anti-ageing therapeutics.

Throughout this study, notable differences in activity were observed between GRE and FRE treatments. Although both GRE and FRE treated ρ^0 3T3-L1 cells exhibited a change in mitochondrial distribution to a more intermediate mitochondrial arrangement, typical of proliferating cells (G1-S or S phase), GRE was ultimately more effective at improving cell growth and proliferation, as illustrated by a decreased population doubling time and attenuation of G1 arrest (Tables 1 and 2). GRE treatment also exhibited greater modulation of glucose utilization and restoration of lactate production, illustrated by an increase in glucose utilization and a decrease in lactate production, relative to ρ^0 control cells. Interestingly however, treatment with FRE exhibited a more prominent effect on mitochondrial health, as shown by the increased $\Delta\Psi_m$, as well a greater capacity to attempt to restore the p-AMPK/AMPK ratio and ATP content relative to wild type cells. This is in accordance with results published on the anti-diabetic properties of rooibos, although an increase in AMPK activation has only been shown in liver and not adipose tissue (Beltrán-Debón et al., 2011; Mazibuko et al., 2015).

Taken together, it is clear that GRE and FRE have different biochemical activities, which can be attributed to their different phytochemical compositions. As reported by Muller et al. (2012) and Mazibuko et al. (2013), GRE had a significantly higher total phenolic content compared to FRE (26.2 and 3.9% respectively), as well as 50.7× more aspalathin, and ± 2× more rutin, iso-rutin and quercetin, all of which are known to be involved in the regulation of glucose uptake and AMPK activation (Mazibuko et al., 2013). Although further investigation into the exact role of individual or combinations of specific polyphenols is still required, this could provide some information with regards to the fact that throughout this study, notable differences in activity were observed between the GRE and FRE treatments. It is important to note however that these results could also suggest that rooibos does not directly target mitochondrial function, the cell would thus become resistant to mitochondrial dysfunction resulting in an improvement in growth kinetics and mitochondrial function.

5. Conclusion

A novel mtDNA depleted (ρ^0) 3T3-L1 preadipocyte cell line representative of the mitochondrial dysfunction observed in preadipocytes during the ageing process was successfully established. Treatment with rooibos extracts, particularly the green extract, exhibit effects which can potentially counteract ageing related insults in preadipocytes which are expected to display mitochondrial dysfunction.

6. Ethics statements

This study did not include any human subjects and animal experiments.

Conflicts of interest

The authors declare no conflicts of interest pertaining to this study.

Acknowledgements

The authors would like to thank Prof E. Joubert of the Agricultural Research Council for supplying the Rooibos extracts, as well as Prof. D. Lang and Mrs. S. Cooper for their guidance with the confocal microscopy imaging at the Confocal and Light Microscope Imaging Facility (University of Cape Town) supported by the Wellcome Trust [108473/Z/15/Z]. This work is based on research supported in part by the Technology and Human Resources for Industry Programme (THRIP), Nelson Mandela University and the South African Rooibos Council (SARC) and the Horace Alfred Taylor Will Trust.

References

Amuthan, G., Biswas, G., Ananadatheerthavarada, H. K., Vijayasarathy, C., Shephard, H. M., & Avadhani, N. G. (2002). Mitochondrial stress-induced calcium signaling, phenotypic changes and invasive behavior in human lung carcinoma A549 cells. *Oncogene, 21*(51), 7839–7849. https://doi.org/10.1038/sj.onc.1205983.

Arakaki, N., Nishihama, T., Owaki, H., Kuramoto, Y., Suenaga, M., Miyoshi, E., ... Higuti, T. (2006). Dynamics of mitochondria during the cell cycle. *Biological & Pharmaceutical Bulletin, 29*(9), 1962–1965. https://doi.org/10.1248/bpb.29.1962.

Arduíno, D. M., Esteves, A. R., Cortes, L., Silva, D. F., Patel, B., Grazina, M., ... Cardoso, S. M. (2012). Mitochondrial metabolism in Parkinson's disease impairs quality control autophagy by hampering microtubule-dependent traffic. *Human Molecular Genetics, 21*(21), 4680–4702. https://doi.org/10.1093/hmg/dds309.

Armand, R., Channon, J. Y., Kintner, J., White, K. A., Miselis, K. A., Perez, R. P., & Lewis, L. D. (2004). The effects of ethidium bromide induced loss of mitochondrial DNA on mitochondrial phenotype and ultrastructure in a human leukemia T-cell line (MOLT-4 cells). *Toxicology and Applied Pharmacology, 196*(1), 68–79. https://doi.org/10.1016/j.taap.2003.12.001.

Arnould, T., Mercy, L., Houbion, A., Vankoningsloo, S., Renard, P., Pascal, T., ... Raes, M. (2003). mtCLIC is up-regulated and maintains a mitochondrial membrane potential in mtDNA-depleted L929 cells. *The FASEB Journal: Official Publication of the Federation of American Societies for Experimental Biology, 17*(14), 2145–2147. https://doi.org/10.1096/fj.03-0075fje.

Ashok, B. T., & Ali, R. (1999). The aging paradox: Free radical theory of aging. *Experimental Gerontology, 34*(3), 293–303. https://doi.org/10.1016/S0531-5565(99)00005-4.

Baret, P., Septembre-Malaterre, A., Rigoulet, M., Lefebvre D'Hellencourt, C., Priault, M., Gonthier, M. P., & Devin, A. (2013). Dietary polyphenols preconditioning protects 3T3-L1 preadipocytes from mitochondrial alterations induced by oxidative stress. *International Journal of Biochemistry and Cell Biology, 45*(1), 167–174. https://doi.org/10.1016/j.biocel.2012.10.007.

Beltrán-Debón, R., Rull, A., Rodríguez-Sanabria, F., Iswaldi, I., Herranz-López, M., Aragonès, G., ... Joven, J. (2011). Continuous administration of polyphenols from aqueous rooibos (Aspalathus linearis) extract ameliorates dietary-induced metabolic disturbances in hyperlipidemic mice. *Phytomedicine, 18*(5), 414–424. https://doi.org/10.1016/j.phymed.2010.11.008.

Brand, M. D., & Nicholls, D. G. (2011). Assessing mitochondrial dysfunction in cells. *Biochemical Journal, 435*(2), 297–312. https://doi.org/10.1042/BJ20110162.

Bratic, A., & Larsson, N. (2013). Review series The role of mitochondria in aging, 123(3). https://doi.org/10.1172/JCI64125.Review.

Buchet, K., & Godinot, C. (1998). Functional F1-ATPase essential in maintaining growth and membrane potential of human mitochondrial DNA-depleted ρ cells. *Journal of Biological Chemistry, 273*(36), 22983–22989. https://doi.org/10.1074/jbc.273.36.22983.

Calabrese, V., Cornelius, C., Dinkova-Kostova, A. T., Iavicoli, I., Di Paola, R., Koverech, A., ... Calabrese, E. J. (2012). Cellular stress responses, hormetic phytochemicals and vitagenes in aging and longevity. *Biochimica et Biophysica Acta – Molecular Basis of Disease, 1822*(5), 753–783. https://doi.org/10.1016/j.bbadis.2011.11.002.

Cartwright, M. J., Tchkonia, T., & Kirkland, J. L. (2007). Aging in adipocytes: Potential impact of inherent, depot-specific mechanisms. *Experimental Gerontology, 42*(6), 463–471. https://doi.org/10.1016/j.exger.2007.03.003.

Chandel, N. S., & Schumacker, P. T. (1999). Cells depleted of mitochondrial DNA (ρ0) yield insight into physiological mechanisms. *FEBS Letters, 454*(3), 173–176. https://doi.org/10.1016/S0014-5793(99)00783-8.

Cottet-Rousselle, C., Ronot, X., Leverve, X., & Mayol, J. (2011). Cytometric assessment of mitochondria using fluorescent probes. *Cytometry Part A, 6*, 405–425.

Das, S., Parveen, S., & Pradhan, A. B. (2014). An insight into the interaction of phenanthridine dyes with polyriboadenylic acid: Spectroscopic and thermodynamic approach. *Spectrochimica Acta – Part A: Molecular and Biomolecular Spectroscopy, 118*, 356–366. https://doi.org/10.1016/j.saa.2013.08.106.

Demine, S., Reddy, N., Renard, P., Raes, M., & Arnould, T. (2014). Unraveling biochemical pathways affected by mitochondrial dysfunctions using metabolomic approaches. *Metabolites, 4*(3), 831–878. https://doi.org/10.3390/metabo4030831.

Dykens, J., Marroquin, L. D., & Will, Y. (2007). Strategies to reduce late-stage drug attrition due to mitochondrial toxicity. *Expert Review of Molecular Diagnostics, 7*(2), 161–175.

Ferree, A., & Shirihai, O. (2012). Mitochondrial oxidative phosphorylation, 748, 13–41. https://doi.org/10.1007/978-1-4614-3573-0.

Finkel, T., & Hwang, P. M. (2009). The Krebs cycle meets the cell cycle: Mitochondria and the G1-S transition. *Proceedings of the National Academy of Sciences of the United States of America, 106*(29), 11825–11826. https://doi.org/10.1073/pnas.0906430106.

Gilkerson, R., Margineantu, D., Capaldi, R., & Selker, J. (2000). Mitochondrial DNA depletion causes morphological changes in the mitochondrial reticulum of cultured human cells. *Federation of European Biochemical Societies (FEBS) Letters, 474*, 1–4.

Gohil, V. M., Sheth, S. A., Nilsson, R., Wojtovich, A. P., Lee, J. H., Perocchi, F., Chen, W., Clish, C. B., et al. (2011). *HHS Public Access, 28*(3), 249–255.

Grüner-Richter, S., Otto, F., Weinreich, B. (2008). Rooibos extract with increased

aspalathin content, process for the preparation of such a rooibos extract, and cosmetic agent containing such a rooibos extract. U.S. Patent Application No. US2008/0247974 A1.
Harman, D. (1972). The biological clock: The mitochondria? *Journal of the American Geriatrics Society, 20*, 145–147.
Holmuhamedov, E., Jahangir, A., Bienengraeber, M., Lewis, L. D., & Terzic, A. (2003). Deletion of mtDNA disrupts mitochondrial function and structure, but not biogenesis. *Mitochondrion, 1*, 13–19.
Joubert, E., & de Beer, D. (2011). Rooibos (Aspalathus linearis) beyond the farm gate: From herbal tea to potential phytopharmaceutical. *South African Journal of Botany, 77*(4), 869–886. https://doi.org/10.1016/j.sajb.2011.07.004.
Kemppainen, E., George, J., Garipler, G., Tuomela, T., Kiviranta, E., Soga, T., ... Jacobs, H. T. (2016). Mitochondrial dysfunction plus high-sugar diet provokes a metabolic crisis that inhibits growth. *PLOS ONE, 11*(1), e0145836. https://doi.org/10.1371/journal.pone.0145836.
Khan, S. M., Smigrodzki, R. M., & Swerdlow, R. H. (2007). Cell and animal models of mtDNA biology: Progress and prospects. *American Journal of Physiology. Cell Physiology, 292*(2), C658–C669. https://doi.org/10.1152/ajpcell.00224.2006.
King, M. P., & Attardi, G. (1989). Human cells lacking mtDNA: Repopulation with exogenous mitochondria by complementation. *Science, 246*, 500–503.
Komulainen, T., Lodge, T., Hinttala, R., Bolszak, M., Pietilä, M., Koivunen, P., Hakkola, J., Poulton, J., et al. (2015). Sodium valproate induces mitochondrial respiration dysfunction in HepG2 in vitro cell model. *Toxicology, 331*, 47–56.
Kukat, A., Kukat, C., Brocher, J., Schäfer, I., Krohne, G., Trounce, I., Villani, G., & Seibel, P. (2008). Generation of rho0 cells utilizing a mitochondrially targeted restriction endonuclease and comparative analyses. *Nucleic Acids Research, 36*, e44.
Kusminski, C. M., & Scherer, P. E. (2012). Mitochondrial dysfunction in white adipose tissue. *Trends in Endocrinology and Metabolism, 23*(9), 435–443. https://doi.org/10.1016/j.tem.2012.06.004.
Lagouge, M., & Larsson, N.-G. (2013). The role of mitochondrial DNA mutations and free radicals in disease and ageing. *Journal of Internal Medicine, 273*(6), 529–543. https://doi.org/10.1111/joim.12055.
Lim, J. H., Lee, J. I., Suh, Y. H., Kim, W., Song, J. H., & Jung, M. H. (2006). Mitochondrial dysfunction induces aberrant insulin signalling and glucose utilisation in murine C2C12 myotube cells. *Diabetologia, 49*(8), 1924–1936. https://doi.org/10.1007/s00125-006-0278-4.
Lui, J. C., Chen, W., Barnes, K. M., & Baron, J. (2010). Changes in gene expression associated with aging commonly originate during juvenile growth. *Mechanisms of Ageing and Development, 131*(10), 641–649. https://doi.org/10.1016/j.mad.2010.08.010.
Magda, D., Lecane, P., Prescott, J., Thiemann, P., Ma, X., Dranchak, P. K., ... Hacia, J. G. (2008). mtDNA depletion confers specific gene expression profiles in human cells grown in culture and in xenograft. *BMC Genomics, 9*(1), 521. https://doi.org/10.1186/1471-2164-9-521.
Margineantu, D., Gregory Cox, W., Sundell, L., Sherwood, S., Beechem, J., & Capaldi, R. (2002). Cell cycle dependent morphology changes and associated mitochondrial DNA redistribution in mitochondria of human cell lines. *Mitochondrion, 1*, 425–435.
Masaki, H. (2010). Role of antioxidants in the skin: Anti-aging effects. *Journal of Dermatological Science, 58*(2), 85–90. https://doi.org/10.1016/j.jdermsci.2010.03.003.
Mazibuko, S. E., Joubert, E., Johnson, R., Louw, J., Opoku, A. R., & Muller, C. J. F. (2015). Aspalathin improves glucose and lipid metabolism in 3T3-L1 adipocytes exposed to palmitate. *Molecular Nutrition and Food Research, 59*(11), 2199–2208. https://doi.org/10.1002/mnfr.201500258.
Mazibuko, S. E., Muller, C. J. F., Joubert, E., De Beer, D., Johnson, R., Opoku, A. R., & Louw, J. (2013). Amelioration of palmitate-induced insulin resistance in C2C12 muscle cells by rooibos (Aspalathus linearis). *Phytomedicine, 20*(10), 813–819. https://doi.org/10.1016/j.phymed.2013.03.018.
Minamikawa, T., Sriratana, A., Williams, D. A., Bowser, D. N., Hill, J. S., & Nagley, P. (1999). Chloromethyl-X-rosamine (MitoTracker Red) photosensitises mitochondria and induces apoptosis in intact human cells. *Journal of Cell Science, 112*(Pt 1), 2419–2430.
Mitra, K., Wunder, C., Roysam, B., Lin, G., & Lippincott-Schwartz, J. (2009). A hyperfused mitochondrial state achieved at G1-S regulates cyclin E buildup and entry into S phase. *Proceedings of the National Academy of Sciences of the United States of America, 106*(29), 11960–11965. https://doi.org/10.1073/pnas.0904875106.
Morton, J. F. (1983). Rooibos tea, *Aspalathus linearis*, a caffeine-less, low-tannin beverage. *Economic Botany, 37*, 164–173.
Muller, C. J. F., Joubert, E., De Beer, D., Sanderson, M., Malherbe, C. J., Fey, S. J., & Louw, J. (2012). Acute assessment of an aspalathin-enriched green rooibos (Aspalathus linearis) extract with hypoglycemic potential. *Phytomedicine, 20*(1), 32–39. https://doi.org/10.1016/j.phymed.2012.09.010.
Page, M. M., Robb, E. L., Salway, K. D., & Stuart, J. A. (2010). Mitochondrial redox metabolism: Aging, longevity and dietary effects. *Mechanisms of Ageing and Development, 131*(4), 242–252. https://doi.org/10.1016/j.mad.2010.02.005.
Park, C. B., & Larsson, N.-G. (2011). Mitochondrial DNA mutations in disease and aging. *The Journal of Cell Biology, 193*(5), 809–818. https://doi.org/10.1083/jcb.201010024.
Park, S. Y., & Lee, W. (2007). The depletion of cellular mitochondrial DNA causes insulin resistance through the alteration of insulin receptor substrate-1 in rat myocytes. *Diabetes Research and Clinical Practice, 77*(3 SUPPL), 165–171. https://doi.org/10.1016/j.diabres.2007.01.051.
Pellegrino, M. W., Nargund, A. M., & Haynes, C. M. (2013). Signaling the mitochondrial unfolded protein response. *Biochimica et Biophysica Acta – Molecular Cell Research, 1833*(2), 410–416. https://doi.org/10.1016/j.bbamcr.2012.02.019.
Pendergrass, W., Wolf, N., & Poot, M. (2004). Efficacy of MitoTracker GreenTM and CMXRosamine to measure changes in mitochondrial membrane potentials in living cells and tissues. *Cytometry Part A, 61*, 162–169.
Queen, B. L., & Tollefsbol, T. O. (2010). Polyphenols and aging. *Current Aging Science, 3*(1), 34–42. https://doi.org/10.2174/1874609811003010034.
Salminen, A., & Kaarniranta, K. (2012). AMP-activated protein kinase (AMPK) controls the aging process via an integrated signaling network. *Ageing Research Reviews, 11*(2), 230–241. https://doi.org/10.1016/j.arr.2011.12.005.
Sanderson, M., Mazibuko, S. E., Joubert, E., De Beer, D., Johnson, R., Pheiffer, C., ... Muller, C. J. F. (2014). Effects of fermented rooibos (Aspalathus linearis) on adipocyte differentiation. *Phytomedicine, 21*(2), 109–117. https://doi.org/10.1016/j.phymed.2013.08.011.
Schroeder, P., Gremmel, T., Berneburg, M., & Krutmann, J. (2008). Partial depletion of mitochondrial DNA from human skin fibroblasts induces a gene expression profile reminiscent of photoaged skin. *Journal of Investigative Dermatology, 128*(9), 2297–2303. https://doi.org/10.1038/jid.2008.57.
Seidel-Rogol, B. L. (2002). Modulation of mitochondrial transcription in response to mtDNA depletion and repletion in HeLa cells. *Nucleic Acids Research, 30*(9), 1929–1934.
Sepe, A., Tchkonia, T., Thomou, T., Zamboni, M., & Kirkland, J. L. (2010). Aging and regional differences in fat cell progenitors – A mini-review. *Gerontology, 57*(1), 66–75. https://doi.org/10.1159/000279755.
Singh, K. K. (2004). Mitochondria damage checkpoint in apoptosis and genome stability. *FEMS Yeast Research, 5*(2), 127–132. https://doi.org/10.1016/j.femsyr.2004.04.008.
Sohal, R. S., & Orr, W. C. (2012). The redox stress hypothesis of aging. *Free Radical Biology and Medicine, 52*(3), 539–555. https://doi.org/10.1016/j.freeradbiomed.2011.10.445.
Stankov, M. V., Lücke, T., Das, A. M., Schmidt, R. E., & Behrens, G. M. N. (2010). Mitochondrial DNA depletion and respiratory chain activity in primary human subcutaneous adipocytes treated with nucleoside analogue reverse transcriptase inhibitors. *Antimicrobial Agents and Chemotherapy, 54*, 280–287.
Tchkonia, T., Morbeck, D. E., Von Zglinicki, T., Van Deursen, J., Lustgarten, J., Scrable, H., ... Kirkland, J. L. (2010). Fat tissue, aging, and cellular senescence. *Aging Cell, 9*(5), 667–684. https://doi.org/10.1111/j.1474-9726.2010.00608.x.
Trifunovic, A., & Larsson, N.-G. (2008). Mitochondrial dysfunction as a cause of ageing. *Journal of Internal Medicine, 263*(2), 167–178. https://doi.org/10.1111/j.1365-2796.2007.01905.x.
van Gisbergen, M. W., Voets, A. M., Starmans, M. H. W., de Coo, I. F. M., Yadak, R., Hoffmann, R. F., ... Lambin, P. (2015). How do changes in the mtDNA and mitochondrial dysfunction influence cancer and cancer therapy? Challenges, opportunities and models. *Mutation Research - Reviews in Mutation Research, 764*, 16–30. https://doi.org/10.1016/j.mrrev.2015.01.001.
Vankoningsloo, S., De Pauw, A., Houbion, A., Tejerina, S., Demazy, C., de Longueville, F., ... Arnould, T. (2006). CREB activation induced by mitochondrial dysfunction triggers triglyceride accumulation in 3T3-L1 preadipocytes. *Journal of Cell Science, 119*(Pt 7), 1266–1282. https://doi.org/10.1242/jcs.02848.
Wallace, D. C. (2005). A mitochondrial paradigm of metabolic and degenerative diseases, aging, and cancer: A dawn for evolutionary medicine. *Annual Review of Genetics, 39*, 359.
Warren, E. B., Aicher, A. E., Fessel, J. P., & Konradi, C. (2017). Mitochondrial DNA depletion by ethidium bromide decreases neuronal mitochondrial creatine kinase: Implications for striatal energy metabolism. *PLoS ONE, 12*(12), 1–22. https://doi.org/10.1371/journal.pone.0190456.
Wilkins, H. M., Carl, S. M., & Swerdlow, R. H. (2014). Cytoplasmic hybrid (cybrid) cell lines as a practical model for mitochondriopathies. *Redox Biology, 2*(1), 619–631. https://doi.org/10.1016/j.redox.2014.03.006.
Yakes, F. M., & Van Houten, B. (1997). Mitochondrial DNA damage is more extensive and persists longer than nuclear DNA damage in human cells following oxidative stress. *Proceedings of the National Academy of Sciences of the United States of America, 94*(2), 514–519. https://doi.org/10.1073/pnas.94.2.514.
Yu, M., Shi, Y., Wei, X., Yang, Y., Zhou, Y., Hao, X., ... Niu, R. (2007). Depletion of mitochondrial DNA by ethidium bromide treatment inhibits the proliferation and tumorigenesis of T47D human breast cancer cells. *Toxicology Letters, 170*(1), 83–93. https://doi.org/10.1016/j.toxlet.2007.02.013.